Available online at www.sciencedirect.com
SCIENCE DIRECT®
Journal of Solid State Chemistry 177 (2004) 1607–1618
JOURNAL OF SOLID STATE CHEMISTRY
http://elsevier.com/locate/jssc

The mixed-valence iron compound $Na_{0.1}Fe_7(PO_4)_6$: crystal structure and ^{57}Fe Mössbauer spectroscopy between 80 and 295 K

G.J. Redhammer,[a,b,*] G. Roth,[a] G. Tippelt,[b] M. Bernroider,[b] W. Lottermoser,[b] and G. Amthauer[b]

[a] *Institute of Crystallography, Technical University (RWTH)-Aachen, Jägerstrasse 17/19, D-52056 Aachen, Germany*
[b] *Institute of Mineralogy, University of Salzburg, Hellbrunnerstr. 34, A-5020 Salzburg, Austria*

Received 1 September 2003; received in revised form 2 December 2003; accepted 14 December 2003

Abstract

The crystal structure of the synthetic iron phosphate $Na_{0.10(1)}Fe_{6.99(1)}(P_{1.00(1)}O_4)_6$ has been refined at 270 and 100 K from single-crystal X-ray diffraction data. The compound is triclinic, $P\bar{1}$, $Z = 1$, lattice parameters: $a = 6.3944(9)$ Å, $b = 7.956(1)$ Å, $c = 9.364(1)$ Å, $\alpha = 105.13(1)°$, $\beta = 108.35(1)°$, $\gamma = 101.64(1)°$ at 270 K and adopts the well-known howardevansite structure type. Iron, being both in the divalent and the trivalent valence state, is ordered on the four symmetry non-equivalent iron positions [Fe^{2+} on Fe(1) and Fe(3), Fe^{3+} on Fe(2) and Fe(4)]. Three of the four iron positions show octahedral oxygen atom coordination, the fourth one, which is occupied by Fe^{2+}, is five-fold coordinated. The structure consists of crankshafts (buckled chains) of edge sharing Fe-oxygen polyhedra, passing through the unit cell in [101] direction. Structural investigation at 100 K shows no change of symmetry. The valence state and distribution of iron was determined by ^{57}Fe Mössbauer spectroscopy. The compound shows 4 subspectra in agreement with the four different Fe sites. The assignment of the Fe^{2+} doublets to the Fe(1) and Fe(3) sites is trivial due to the 2:1 stoichiometry, also found in the Mössbauer spectra. For the Fe^{3+} sites, the temperature-dependent variation of structural distortion parameters and the quadrupole splitting led to a clear doublet assignment.

Keywords: Iron phosphate; Structure determination; ^{57}Fe Mössbauer spectroscopy; Mixed valence compound; Howardevansite structure type

1. Introduction

Compounds, which contain iron in both valence states Fe^{2+} and Fe^{3+} are of special interest as these materials can show electron delocalization at elevated temperatures. As stated by Amthauer and Rossman in 1982, a basic requirement for this is the presence of infinite structural units (e.g., octahedra), which are connected—at least—by edges [1]. Materials showing such effects are, among others, the minerals magnetite Fe_3O_4 [2], ilvaite [3,4] or libscombite, nominally $Fe^{2+}Fe_2^{3+}(PO_4)_2(OH)_2$ [5]. Libscombite is most probably the partly oxidized high temperature form of the mineral barbosalite $Fe^{2+}Fe_2^{3+}(PO_4)_2(OH)_2$ [6, Redhammer, preliminary results]. In the context of research on phosphate minerals having iron in both the di- and the trivalent state, experiments have been performed to grow the lazulite type compounds barbosalite and lipscombite using hydrothermal techniques ($400°C < T < 700°C$, $P = 0.2-0.4$ GPa).

In several of these experiments, large, black idiomorphic crystals were obtained. Preliminary X-ray diffraction experiments (powder diffraction, auto-indexing) on crushed single crystals have shown the compound to have a triclinic unit cell, space group $P\bar{1}$. While searching the Inorganic Crystal Structure Database (ICSD) for these data, a compound having the chemical composition $Fe_7(PO_4)_6$ was found, fitting the symmetry and unit cell parameters, determined for the black crystals, rather well. $Fe_7(PO_4)_6$ at 295(2) K was first reported by Grobunov and co-workers [7], however, topological details of the structure are hard to obtain as the original literature is in Russian and not easily available. Furthermore, the topological description of

*Corresponding author. Neuhofen 224/TOP 1, A-4910 Ried im Innkreis, Austria. Fax: +436628044622.
E-mail address: guenther.redhammer@aon.at (G.J. Redhammer).

0022-4596/$ - see front matter © 2003 Elsevier Inc. All rights reserved.
doi:10.1016/j.jssc.2003.12.016

the structure in Ref. [7] is rather rudimentary. $Fe_7(PO_4)_6$ is isotypic with the vanadate howardevansite $NaCu^{2+}Fe_2^{3+}(VO_4)_3$ [8]. A series of synthetic compounds are known to exhibit this howardevansite structure type, among them vanadates such as $LiCuFe_2(VO_4)_3$ [9] or β-$Cu_3Fe_4(VO_4)_6$ [10], molybdates such as $Ag_2Zn_2(MoO_4)_3$ [11] and $NaMg_5(MoO_4)_6$ [12] and phosphates. Among the isotypic iron phosphates the compounds $Ni_3Fe_4(PO_4)_6$ [13], $Co_3Fe_4(PO_4)_6$ [14,15], $Mn_2FeFe_4(PO_4)_6$ [15] and $Cu_{3-x}Fe_{4+x}(PO_4)_6$ [16] are known.

Here we present a re-determination of the structure of this iron phosphate at 100 and 270 K which is complemented by a full description of its ^{57}Fe-Mössbauer spectrum at temperatures between 80 and 295 K.

2. Experimental

2.1. Synthesis and material-chemistry

Starting material for the synthesis of the title compound was a fine-grained powder of synthetic barbosalite $Fe^{2+}Fe_2^{3+}(PO_4)_2(OH)_2$. The latter was synthesized by a wet chemical method following the description of Vochten and DeGrave [17]. NaH_2PO_4, $FeSO_4 \cdot 2H_2O$ and $Fe(NO)_3 \cdot 7H_2O$ were used as starting materials. 0.1 M aqueous solutions of the above-mentioned compounds were added simultaneously to boiling water at a rate of $\approx$200 mL/h. The reaction mixture was then kept at boiling temperature for additional 24 h, during which the crystalline phase was formed. Other than Ref. [17], we obtained synthetic barbosalite instead of libscombite. The barbosalite, synthesized as described above, contained some traces of NaH_2PO_4 as an impurity phase. To investigate the thermal stability of barbosalite, several experiments were performed for which about 500 mg of the sample material were filled—together with $\approx$50 μL distilled H_2O—into $Ag_{70}Pd_{30}$ tubes, inner diameter 2.8 mm. The tubes were welded tight, and placed into larger Au-tubes containing a solid-state oxygen buffer (nickel/nickeloxide = NNO) to control the oxygen fugacity. This tube-in-tube technique is described in detail in Ref. [18]. The so prepared sample containers were put into a standard cold-sealed hydrothermal apparatus (externally heated, cold sealed Tuttle type pressure vessels) and maintained at temperatures between 673 and 973 K and at a pressure of 0.4 GPa for a total of three weeks. Within the temperature range 673–723 K, the initial barbosalite starting material reacted to a coarse-grained product, showing idiomorphic crystals of the title compound. An experiment at 773 K showed a mixture of the black iron-phosphate and pale pink colored transparent crystals, which turned out to be $Fe_2^{2+}P_2O_7$ (triclinic, P-1), experiments at and above 823 K revealed the pale pink product only. The crystals, used in this study are those, grown at 723 K and a pressure of 0.4 GPa. The compound $Fe_2P_2O_7$ will be described elsewhere (Redhammer and Roth, in preparation).

Fig. 1 displays a scanning electron microscopy image of an aggregate of crystals of the title compound. Individual crystals were up to 1.5 mm in size. Qualitative energy dispersive X-ray analysis (EDX) on some of these crystals showed the presence of small amounts of sodium.

In order to exactly determine the chemical composition of the title compound, several of the crystals were embedded in epoxy-resin, polished, covered with carbon and analyzed with a JEOL JXA 8600 electron microprobe (acceleration voltage 15 kV, initial beam current 40 nA, beam focused to 5 μm). NaCl, FeO and a natural apatite were used as standards. Twenty single point analyses at random positions in various grains and two lines, 18 measuring points each, rim–core–rim, were performed. The two line measurements show that the phosphorus and the iron content are very constant, but the sodium content varies to some extent (0.25–0.35 wt%). Results of individual spot and line-measurements were merged and gave the following chemical composition (wt% = weight percent): 0.32(6) wt% Na_2O, 53.30(8) wt% FeO and 42.62(8) wt% P_2O_5. Based on 24 oxygen atoms and the Fe^{2+}/Fe^{3+} ratio as determined by Mössbauer spectroscopy, the chemical formula of the title compound calculates to $Na_{0.10(2)}Fe^{2+}_{3.11(1)}Fe^{3+}_{3.88(1)}(P_{1.00(1)}O_4)_6$. The compound is fully balanced in charge (48 positive to 48 negative charges). Even if there are some variations in the Na-content, the variations within a grain and from grain to grain are small and chemical homogenity can be assumed. The presence of sodium originates from the presence of a small amount of NaH_2PO_4 in the synthetic barbosalite, used as starting material for synthesis.

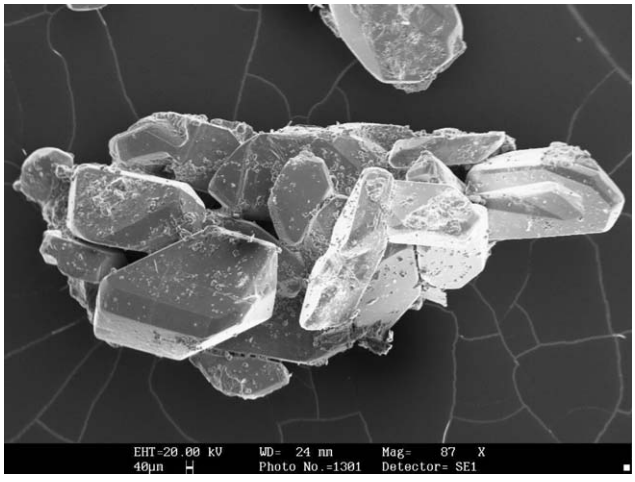

Fig. 1. Scanning electron microscopy image of an aggregate of crystals of the title compound (723 K, 0.4 GPa). The SEM picture kindly was taken by Dr. Gertrude Friedl (Univ. Salzburg).

2.2. Single-crystal X-ray diffraction

A black, cuboid fragment of the title compound ($0.16 \times 0.8 \times 0.7$ mm, formula weight 963.07 g/mol, density 3.85 mg/m^3, absorption coefficient 6.67 mm^{-1} for Mo$K\alpha$ radiation) was used for single-crystal X-ray diffraction experiments. Intensity data sets were collected at 100 and 270 K on a Stoe IPDS II imaging-plate diffractometer system using the rotation method (Mo$K\alpha$ radiation, pyrolytic graphite monochromator). The system is equipped with a cryo-stream liquid N_2-cryostat (85–300 K, accuracy at least 1 K). Intensity data were collected up to 65.0° in 2θ within an ω-range of 0–180° and two different φ positions (15° and 110°); the ω rotation during imaging was 1.5°/frame. Lattice parameters were determined from single-crystal X-ray diffraction data using 8017 (100 K) and 8210 (270 K) Bragg reflexions. Absorption correction was done empirically via equivalents using the SHAPE-software [19]. Structure solution (using Patterson methods) and subsequent refinement was carried out with the programs SHELXS-97 [20] and SHELXL-97 [21] as implemented in the program suite WinGX 1.64 [22]. X-ray scattering factors in their ionic form, together with anomalous dispersion coefficients were taken from the International Tables for Crystallography [23]. The program DIAMONDS 2.0 [24] was used to prepare the graphical visualization of the crystal structure.

2.3. ^{57}Fe Mössbauer spectroscopy

Transmission ^{57}Fe Mössbauer spectra between 80 and 700 K were collected using a Mössbauer apparatus in horizontal arrangement (^{57}Co/Rh single line thin source, constant acceleration, symmetric triangular velocity shape, multi-channel analyser with 1024 channels, and velocity calibration to α-Fe). The Mössbauer spectrometer is equipped with an evaporation-cryostat for low- and with an in-house-designed furnace for high-temperature measurements. For Mössbauer absorber preparation, samples were carefully ground under ethanol (to avoid oxidation), mixed with epoxy resin (low temperature measurements) and filled into Cu-rings (inner diameter 10 mm), covered with a high-purity Al-foil on one side. The folded spectra were analyzed using classical Hamiltonian site analysis (using Lorentzian shaped doublets), as implemented in the program suite RECOIL. Complete thickness correction was applied to all Mössbauer spectra before analysis [25–27].

3. Results and discussion

3.1. Structure determination

Table 1 contains crystal data and details on data collection and structure refinement for both, the 270 and 100 K measurements, Table 2 gives fractional atomic coordinates and equivalent isotropic atomic displacement parameters and Table 3 compiles selected geometric and distortion parameters for the title compound. The intensity data set collected at 270 K was used to build up the structural model. Indexing of the data and the analysis of the systematic absences supports the assignment of the centric space group P-1. Intensity statistics yielded $|E^2 - 1| = 1.018$, close to the expected value of 0.968 for centrosymmetric structures. Structure solution in P-1 using Patterson methods [20] yields seven atomic positions which could be identified as four symmetrically independent iron positions and three symmetry independent phosphorus positions. Oxygen atom positions were found by inspection of the difference electron density map after the first refinement

Table 1
Structural parameters and details of data collection and refinement for $Na_{0.10}Fe^{2+}_{3.11}Fe^{3+}_{3.88}(PO_4)_6$ at 270 and 100 K

	270 K	100 K
Crystal data		
Cell setting, space group	Triclinic, P-1	Triclinic, P-1
a(Å)	6.3944 (9)	6.3911 (9)
b(Å)	7.9562 (11)	7.9499 (11)
c(Å)	9.3643 (13)	9.3586 (13)
α(deg)	105.133 (11)	105.128 (11)
β(deg)	108.353 (11)	108.354 (11)
γ(deg)	101.637 (11)	101.692 (11)
V(Å^3)	415.01 (10)	414.08 (10)
Z	1	1
Range (deg)	2.1–32.1	2.5–32.1
Data collection		
Absorption correction	Numerical	Numerical
T_{min}	0.34	0.34
T_{max}	0.43	0.43
No. of measured reflections	8106	8080
No. of independent reflections	2844	2839
No. of observed reflections	2447	2447
Completeness of data	97.8%	97.4%
Criterion for observed reflections	$I > 2\sigma(I)$	$I > 2\sigma(I)$
R_{int}	4.02%	3.99%
θ_{max} (deg)	32.1	32.1
Range of h, k, l	$-9 \rightarrow h \rightarrow 9$	$-9 \rightarrow h \rightarrow 9$
	$-11 \rightarrow k \rightarrow 11$	$-11 \rightarrow k \rightarrow 11$
	$-12 \rightarrow l \rightarrow 13$	$-12 \rightarrow l \rightarrow 13$
Refinement		
Refinement on	F^2	F^2
Final R indices [$I > 2\sigma(I)$]	$R_1 = 2.29\%$,	$R_1 = 2.23\%$
	$wR_2 = 4.70\%$	$wR_2 = 4.70\%$
Final R indices (all data)	$R_1 = 3.07\%$	$R_1 = 2.86\%$
	$wR_2 = 4.89\%$	$wR_2 = 4.87\%$
Goodness-of-fit S	1.040	1.049
No. of parameters	180	180
Weighting scheme (a/b)	0.0264/0.0303	0.0264/0.0303
$(\Delta/\sigma)_{max}$	0.001	0.001
$\Delta\rho_{max}$, $\Delta\rho_{min}$(e/Å^3)	0.465, −0.559	0.504, −0.594
Extinction correction method	SHELXL	SHELXL
Extinction coefficient	0.0270 (13)	0.0227 (13)

Calculated $w = 1/[\sigma^2(F_o^2) + (aP)^2 + bP]$ where $P = (F_o^2 + 2F_c^2)/3$.

Table 2
Atomic coordinates and equivalent isotropic displacement parameters (Å^2) for $Na_{0.10}Fe^{2+}_{3.11}Fe^{3+}_{3.88}(PO_4)_6$ at 270 and 100 K.

	x	y	z	U_{eq} (Å^2)
270 K				
Fe(1)	1/2	1/2	1/2	0.0083(1)
Fe(2)	0.5441(1)	0.2202(1)	0.0252(1)	0.0059(1)
Fe(3)	0.7792(1)	0.3116(1)	0.7846(1)	0.0073(1)
Fe(4)	0.1180(1)	0.0480(1)	0.3902(1)	0.0060(1)
P(3)	0.2715(1)	0.3508(1)	0.7313(1)	0.0046(1)
P(2)	0.5916(1)	0.0927(1)	0.3323(1)	0.0048(1)
P(1)	0.0966(1)	0.2665(1)	0.1259(1)	0.0068(1)
O(1)	0.0434(3)	0.1289(2)	0.2068(2)	0.0149(3)
O(2)	0.2252(2)	0.4556(2)	0.2573(2)	0.0102(2)
O(3)	0.2416(3)	0.2119(2)	0.0314(2)	0.0161(3)
O(4)	−0.1337(2)	0.2651(2)	0.0056(2)	0.0103(3)
O(5)	0.3763(2)	−0.0342(2)	0.3357(2)	0.0076(2)
O(6)	0.6151(2)	0.2882(2)	0.4168(2)	0.0123(3)
O(7)	0.8065(2)	0.0402(2)	0.4140(2)	0.0079(2)
O(8)	0.5639(2)	0.0510(2)	0.1542(2)	0.0082(2)
O(9)	0.2933(2)	0.5516(2)	0.7950(2)	0.0116(3)
O(10)	0.2749(2)	0.3033(2)	0.5610(2)	0.0080(2)
O(11)	0.4794(2)	0.3126(2)	0.8419(2)	0.0079(2)
O(12)	0.0444(2)	0.2357(2)	0.7269(2)	0.0074(2)
Na	0	1/2	1/2	0.027(3)
100 K				
Fe(1)	1/2	1/2	1/2	0.0051(1)
Fe(2)	0.5441(1)	0.2198(1)	0.0248(1)	0.0036(1)
Fe(3)	0.7791(1)	0.3119(1)	0.7847(1)	0.0041(1)
Fe(4)	0.1176(1)	0.0476(1)	0.3903(1)	0.0037(1)
P(3)	0.2713(1)	0.3510(1)	0.7312(1)	0.0031(1)
P(2)	0.5912(1)	0.0925(1)	0.3321(1)	0.0032(1)
P(1)	0.0967(1)	0.2665(1)	0.1259(1)	0.0049(1)
O(1)	0.0425(2)	0.1281(2)	0.2060(2)	0.0114(3)
O(2)	0.2256(2)	0.4553(2)	0.2578(2)	0.0069(2)
O(3)	0.2423(2)	0.2124(2)	0.0308(2)	0.0123(3)
O(4)	−0.1339(2)	0.2654(2)	0.0053(2)	0.0076(2)
O(5)	0.3762(2)	−0.0347(2)	0.3358(1)	0.0051(2)
O(6)	0.6155(2)	0.2883(2)	0.4168(2)	0.0084(2)
O(7)	0.8065(2)	0.0400(2)	0.4138(2)	0.0055(2)
O(8)	0.5635(2)	0.0507(2)	0.1537(2)	0.0058(2)
O(9)	0.2928(2)	0.5521(2)	0.7943(2)	0.0085(3)
O(10)	0.2748(2)	0.3032(2)	0.5606(1)	0.0052(2)
O(11)	0.4799(2)	0.3133(2)	0.8418(2)	0.0055(2)
O(12)	0.0442(2)	0.2356(2)	0.7269(1)	0.0047(2)
Na	0	1/2	1/2	0.014(3)

U_{eq} is defined as one-third of the trace of the orthogonalized U_{ij} tensor.

Table 3
Selected bond lengths (Å) and polyhedral distortion parameters of $Na_{0.10}Fe^{2+}_{3.11}Fe^{3+}_{3.88}(PO_4)_6$

	270 K	100 K
Fe1–O6 × 2	2.041(1)	2.041(1)
Fe1–O10 × 2	2.219(1)	2.215(1)
Fe1–O2 × 2	2.279(1)	2.272(1)
⟨Fe1–O⟩	*2.179*	*2.176*
⟨O–O⟩	*3.082*	*3.077*
BLD (%)	4.24	4.14
OAV (deg)	27.10	26.71
OQE	1.0116	1.0113
Volume (Å^3)	13.61	13.55
Fe2–O9	1.938(1)	1.937(1)
Fe2–O3	1.942(1)	1.939(1)
Fe2–O11	1.999(1)	2.000(1)
Fe2–O8	2.027(1)	2.023(1)
Fe2–O4	2.093(1)	2.090(1)
Fe2–O8	2.175(1)	2.166(1)
⟨Fe2–O⟩	*2.029*	*2.026*
⟨O–O⟩	*2.866*	*2.863*
BLD	3.46	3.36
OAV	68.07	68.39
OQE	1.0220	1.0221
Volume (Å^3)	10.80	10.76
Fe3–O2	1.995(1)	1.996(1)
Fe3–O5	2.059(1)	2.055(1)
Fe3–O12	2.086(1)	2.086(1)
Fe3–O4	2.118(1)	2.113(1)
Fe3–O11	2.148(1)	2.143(1)
⟨Fe3–O⟩	*2.081*	*2.079*
⟨O–O⟩	*3.102*	*3.098*
BLD	2.08	2.04
Volume (Å^3)	6.99	6.95
Fe4–O1	1.944(1)	1.948(1)
Fe4–O10	2.040(1)	2.038(1)
Fe4–O5	2.052(1)	2.053(1)
Fe4–O7	2.063(1)	2.059(1)
Fe4–O7	2.082(1)	2.080(1)
Fe4–O12	2.103(1)	2.096(1)
⟨Fe4–O⟩	*2.047*	*2.046*
⟨O–O⟩	*2.884*	*2.881*
BLD	1.80	1.72
OAV	70.23	69.23
OQE	1.0206	1.0203
Volume (Å^3)	11.11	11.08
P3–O9	1.512(1)	1.514(1)
P3–O12	1.534(1)	1.534(1)
P3–O11	1.546(1)	1.547(1)
P3–O10	1.549(1)	1.551(1)
⟨P3–O⟩	*1.535*	*1.536*
⟨O–O⟩	*2.507*	*2.509*
BLD	0.79	0.81
TAV	0.55	0.65
TQE	1.0003	1.0003
Volume (Å^3)	1.86	1.86
P2–O6	1.502(1)	1.502(1)
P2–O7	1.545(1)	1.546(1)
P2–O5	1.549(1)	1.548(1)
P2–O8	1.557(1)	1.559(1)
⟨P2–O⟩	*1.538*	*1.539*
⟨O–O⟩	*2.5106*	*2.5116*
BLD	1.17	1.20
TAV	7.24	7.20
TQE	1.0018	1.0018
Volume (Å^3)	1.86	1.87
P1–O3	1.520(1)	1.525(1)
P1–O1	1.527(1)	1.527(1)
P1–O2	1.533(1)	1.532(1)
P1–O4	1.543(1)	1.546(1)
⟨P3–O⟩	*1.531*	*1.533*
⟨O–O⟩	*2.500*	*2.502*
BLD	0.47	0.43
TAV	2.80	2.96
TQE	1.0007	1.0008
Volume (Å^3)	1.84	1.85

cycles. A total of 12 different oxygen atom positions were found subsequently. After anisotropic refinement of all the non-symmetry equivalent atoms, a residual electron density of 4.92 e/Å^3 was left at position 0, $\frac{1}{2}$, $\frac{1}{2}$. As the only possible residual element, which could be present in the structure, is sodium, this element was put on this position and the occupancy was allowed to vary freely. This removed the large residual electron density peak and yields a smooth difference electron density map with the largest difference peak/hole being smaller than 0.6 e Å^3. The occupation of the Na position refined to 0.122(9) (with 1 corresponding to a fully occupied site). This corresponds to 0.122(9) Na atoms per formula unit and is in good agreement with the chemical composition found by electron microprobe analysis (0.10 Na). Furthermore, the occupations of the Fe positions also have been allowed to vary. They converged to values corresponding to fully occupied sites (0.995–1.002), thus in the final refinements they were fixed again on their ideal values.

3.2. Structural topology at 270 K

The crystal structure of the title compound consists of isolated PO_4-tetrahedra and four different types of Fe-polyhedra. The Fe(1) atom located at the center of the unit cell on a point of inversion is coordinated by six oxygen atoms forming an octahedral site and is occupied by ferrous iron. As will be shown below, ^{57}Fe Mössbauer spectroscopy can be used as a definite proof for this assignment, but also the bond valence sum [29] at the Fe(1)-site with 1.87 valence units (v.u.) gives a hint that the site is occupied by Fe^{2+} only. The individual Fe(1)–O bond lengths range between 2.041(1) and 2.279(1) Å. The average Fe1–O value is 2.179 Å, which is—by far—the largest value among all the four Fe-sites. The deviation of individual bond lengths from their mean value (BLD, [28]) amounts 4.24%, which is a rather high value. The quadratic octahedral angle variance [28] is also rather large (OAV = 27.10°) and shows that Fe1 occupies a distorted site. The average O–O edge length within the Fe1 site is 3.082 Å and the polyhedral volume calculates to 13.606 Å^3. Among all, the Fe(1)O_6 octahedron is the largest of all polyhedra in the compound. All of the six octahedral corners are shared with PO_4 tetrahedra (Fig. 2a). Additionally, the O(10) oxygen atom is not only part of the Fe(1)O_6 octahedron and the P(3)O_4-tetrahedron, but also is part of the Fe(4)-octahedron; the O(6) oxygen atom belongs to the Fe(1)O_6-, the P(1)O_4- and the Fe(3)O_5-site. The Fe(2)-site also is coordinated by six oxygen atoms, forming an octahedral site which is occupied by ferric iron. The bond valence sum at the Fe(2) site was calculated to be 2.96 valence units, close to the valence of ferric iron. The individual Fe(2)–O bond lengths range between 1.938(1) and 2.175(1) Å, the average Fe(2)–O bond length is 2.029 Å, which is shorter than the average Fe(1)–O 0.15 Å, which is close to the difference in ionic radius between $^{VI}Fe^{2+}$ (0.78 Å) and $^{VI}Fe^{3+}$ (0.645 Å). Ionic radii are taken from Ref. [30] and the superscript roman number refers to the coordination number of the cation. Along with Fe(2)–O bond lengths, the average O–O edge lengths at the Fe(2) site are distinctly shorter (average O–O = 2.866 Å). The same applies to the octahedral volume with 10.804 Å^3. In terms of the bond length distortion, the Fe(2) site appears to be closer to the geometry of an ideal octahedron than the Fe(1) site, however, the quadratic octahedral angle variance [28] is much larger with OAV = 68.07°. The octahedral quadratic elongation (OQE, [28]) is 1.0220 for the Fe(2) site as compared to 1.0116 for the Fe(1) site, i.e. the Fe(1) site appears to be more ideal. Each corner of the Fe(2) octahedron is—at the same time—a corner of one PO_4 tetrahedron (Fig 2b). In addition to the connection with the tetrahedral sites, a Fe(2) octahedron shares one common edge (O8–O8 edge) with another Fe(2) octahedron in "*cis*"-configuration and one common edge with a Fe(3) site via the O4–O11 edge being in "*trans*" configuration. It is the O8–O8 and the O4–O11 edge, which represent the two shortest O–O interatomic distances [2.586(1) and 2.628(1) Å, respectively] and the smallest O–Fe(2)–O bond angles [75.9(1)° and 79.9(1)°, respectively]. These small values are due to increased electrostatic repulsive forces between highly charged cations (Fe^{2+} and Fe^{3+}) across the common edge. Decreasing the O–Fe–O bond angle opposite to the

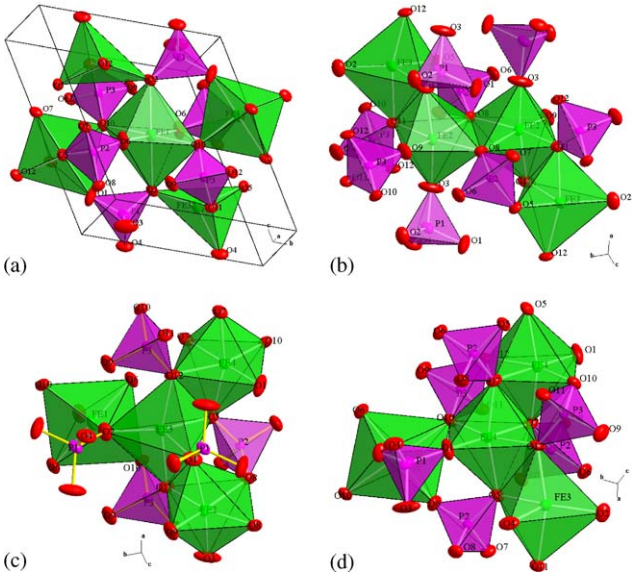

Fig. 2. Polyhedral representation of the nearest environments around a central Fe-site (a) Fe(1) site, (b) Fe(2) site, (c) Fe(3) site, two of the PO_4 tetrahedra are not displayed as polyhedra for clarity, (d) Fe(4) site. Orientations are different from each other in order to better show interconnection between different sites.

common edge, which goes along with decreasing the O–O interatomic distances, brings the two highly charged cations further apart. There are no connections to the other Fe-sites other than Fe(2) and Fe(3) sites. The Fe(3) site is surrounded only by five oxygen atoms, forming a trigonal bi-pyramid. Bond valence sum calculations [28] yield a value of 1.97 valence units suggesting that the Fe(3) site is occupied by divalent iron. It was also stated in Ref. [7], that the 5-fold coordinated site is occupied by Fe^{2+}. This site thus represents the rare case of ferrous iron being in a 5-fold coordination. The bond lengths at the Fe(3)-site range between 1.995(1) and 2.148(1) Å with a mean value of 2.081 Å.The average O–O edge length is 3.102 Å and the polyhedral volume amounts to 6.978 $Å^3$, which is, due to the 5-fold coordination, by far the smallest of all the four Fe polyhedra. As for the Fe(1) and Fe(2) sites, all the corners of the Fe(3)-polyhedron are shared with PO_4 tetrahedra. The O4–O11 edge (Fig. 2c) is common to the Fe(2) octahedron and the trigonal Fe(3)-bi-pyramid, the O5-O12 edge is shared by the Fe(4) and Fe(3) sites. Again, the two common edges are those with the smallest O–O interatomic distances [2.628(1) and 2.632(1) Å, respectively]. The smallest O–Fe(3)–O bond angles are those opposite to the common edges.

The Fe(4) atom is coordinated by six oxygen atoms, forming an octahedral site. The Fe(4) position is occupied by ferric iron (bond valence sum = 2.78 valence units [28]) and the six different Fe(4)–O bond lengths vary between 1.944(1) and 2.103(1) Å, mean value 2.047 Å. The Fe(4) octahedron is rather similar to the Fe(2) octahedron with the polyhedral volume ($V = 11.106\ Å^3$) and the quadratic octahedral angle variance (OAV = 70.22°) being slightly larger than for $Fe(2)O_6$. The bond length distortion BLD amounts to 1.80% and is about half the value for the Fe(2) octahedron, whereas the octahedral quadratic elongation is very similar for both sites. The Fe(4) octahedron shares all of its corners with PO_4 tetrahedra. A common edge (O5–O12) connects the Fe(4) octahedron in "*trans*" configuration with the Fe(3) site, another common edge connects the Fe(4) site with another Fe(4) site via the O7–O7 edge ("trans" configuration).

As can be seen from Fig. 2, the Fe(2), Fe(3) and Fe(4) sites are connected to each other by common edges, thereby forming an infinite crankshaft-like buckled chain, which has a stacking sequence of Fe(3)–Fe(2)–Fe(2)–Fe(3)–Fe(4)–Fe(4)–Fe(3)–Fe(2)–Fe(2)⋯ (Fig. 3). The connection of individual polyhedra for the above mentioned sequence is C–T–C–T–C⋯ with C = *cis* and T = *trans*. The only *trans* connection is the one between Fe(2)–Fe(2). Within a chain, Fe^{2+} and Fe^{3+} are strictly ordered and have a ratio of 1:2, where pairs of Fe^{3+} are interrupted by Fe^{2+} atoms. The Fe–Fe cationic distances within the chains range between 3.065(1) Å [Fe(4)–Fe(4)] and 3.314(1) Å [Fe(2)–Fe(2)]. Both the shortest and largest Fe–Fe interatomic distances belong to Fe^{3+}–Fe^{3+} pairs, the distances between Fe^{2+} and Fe^{3+} range between 3.208(2) and 3.226(1)Å. Because of the rather long interatomic distances and the ordered arrangement of Fe^{2+} and Fe^{3+} it is assumed that no thermally induced electron charge transfer (electron hopping) at elevated temperatures will take place.

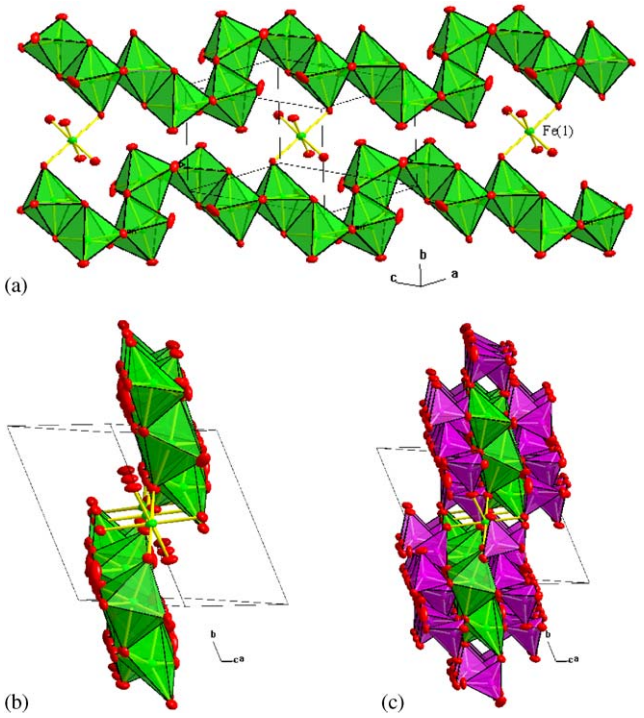

Fig. 3. Polyhedral representation of two of the four infinite chains of Fe-polyhedra, passing through the unit cell, in different orientations (a, b). In (c) PO_4 tetrahedra are added.

Two of these chains pass through the unit cell in [101] direction and are related to each other via the center of inversion at $(\frac{1}{2}, \frac{1}{2}, \frac{1}{2})$. The chains are bridged by the Fe(1) octahedron [with Fe(1) at the center of inversion], which shares corners with the Fe(3) and the Fe(4) sites. Fig. 3 shows two of these chains in different orientations.

The space between the Fe-polyhedra is filled by PO_4 tetrahedra (Fig. 3c) which form walls, separating the different chains of Fe-polyhedra from each other. The PO_4 tetrahedra are similar in size with the P–O bond lengths ranging between 1.502(1) and 1.557(1) Å (mean values ranging between 1.531 Å and 1.538 Å) and the tetrahedral volume lies between 1.839 $Å^3$ and 1.863 Å. However, there are differences in the geometric environment and polyhedral distortion between the three different PO_4 units. The most regular tetrahedral oxygen coordination is found around the P(3) phosphorus atom. Here the quadratic tetrahedral angle variance [28] amounts to 0.54°, the bond length distortion BLD = 0.79% and the tetrahedral quadratic elongation [28] TQE = 1.0003. The $P(3)O_4$ tetrahedron shares corners with a total of 7 nearest Fe polyhedra, 1 with

the Fe(1) octahedron, and 2 with each of the Fe(2), Fe(3) and Fe(4) sites. The most distorted tetrahedron is the one around the P(2) atom. Here the TAV is 7.24°, the BLD = 1.17% and the TQE amounts to 1.0018. The $P(2)O_4$ tetrahedron also shares its corners with a total of 7 nearest Fe sites, among them are 3 different Fe(4) sites, two Fe(2) sites and one Fe(3) and Fe(1) site, respectively.

Sodium is located in a cavity of the structure and is surrounded by six oxygen atoms having bond lengths between 2.437(2) and 2.673(2) Å. The Na atom shows large anisotropic atomic displacement parameters (see Table 2) which can be seen as an indication of positional disorder or a split position off the center of the cavity at $(\frac{1}{2},0,\frac{1}{2})$. However, it was not possible to refine such a split position both at 270 K and at 100 K. It is assumed that the incorporation of sodium has no direct influence onto the geometries and distortion environments of the individual polyhedra described above. However, sodium obviously is necessary to balance charges. As Mössbauer spectroscopy has shown, there is slightly less ferric iron found than would be expected for the iron compound having ideal 3:4 stoichiometry for Fe^{2+}:Fe^{3+}. This deficit in positive charge is balanced by the incorporation of a small amount of sodium.

3.3. Structure at 100 K

At 100 K, the structure of the title compound was found to show the space group *P*-1, too, and the structure at low temperatures is very similar to the one at 270 K. Structural parameters, details on refinement, atomic coordinates and selected bond lengths and angles at 100 K are included in Tables 1–3. Upon cooling, the lattice parameters decrease by about 0.05–0.08%. From that data, linear thermal expansion coefficients can be estimated for *a*, *b* and *c* to take values of 1.9(5), 3.7(5) and $3.3(5)\times10^{-5}\,K^{-1}$, respectively. Mean Fe–O bond lengths decrease by $\approx$0.003 Å ($\approx$0.13%) between 270 and 100 K, the volume of the Fe-polyhedra shrinks by $\approx$0.4%, with the exception of the Fe(4) octahedron, which decreases by 0.2% only. However, it is not generally true, that all individual bond lengths also decrease uniformly with decreasing temperature. There are also some bond lengths, e.g., Fe2−O11, which increase with decreasing temperature. The Fe(1)-octahedron appears to be somewhat more regular at 100 K as compared to 270 K as both, the BLD and the OAV, decrease with decreasing temperature. For the $Fe(2)O_6$ octahedron, a small increase of the octahedral angle variance is observed with decreasing *T*, whereas for the $Fe(4)O_6$ octahedron, the OAV decreases with decreasing *T*, i.e. the latter Fe^{3+} site appears to be slightly more regular at lower temperatures. This effect has some importance for the interpretation of the ^{57}Fe Mössbauer spectra of the title compound. Tetrahedral sites normally appear as rigid units upon changes in a parameter of state (temperature, pressure). One would expect that decreasing temperature decreases bond and edge lengths and polyhedral volume. However, this is actually not the case for the PO_4 tetrahedra in the title compound. For all of the three tetrahedra, the average P–O bond lengths as well as the average O–O edge lengths are larger at 100 K, together with the polyhedral volume, as compared to 270 K. The anisotropic atomic displacement parameters are about 20% smaller than at 270 K.

3.4. Comparison with other howardevansite type Fe-phosphates

In the following, we will—in brief—compare the title compound with previously published phosphates, isotypic to $Na_{0.1}Fe_7(PO_4)_6$. It has to be noted that for the iron containing compounds only the data for $Ni_3Fe_4(PO_4)_6$ were obtained from single-crystal X-ray diffraction, the data for $(Me^{2+}Fe^{3+})_7(PO_4)_6$, $Me = Co^{2+}$, Cu^{2+} and Mn^{2+} were extracted from Rietveld profile refinement of powder diffraction data [14–16]. The structural parameters of the latter are much less precise than the one obtained from single crystals. Furthermore, the data on $Na_{0.1}Fe_7(PO_4)_6$ presented in this study are much more precise than the one of [7], i.e. the estimated standard deviations are smaller by a factor of at least 10. Basic structural parameters (lattice parameters and atomic coordinates) for the isotypic howardevansite type compounds given in Table 4 have been extracted from the Inorganic Crystal Structure Database (ICSD). Using these data, average bond lengths, polyhedral volumes and distortion parameters have been calculated, which are, together with their references, also listed in Table 4.

In terms of the octahedral angle variance OAV [28], the *M*(1) site, which contains the divalent cations in the octahedral oxygen atom coordination, is the most regular *M* site out of the four. With OAV = 27.1° and a bond lengths distortion of 4.2%, the title compound exhibits one of the most ideal *M*(1) sites among the anhydrous orthophosphates given in Table 4. Similar distortions are revealed by the *M*(1) site in $Me_3Fe_4(PO_4)_6$, $Me = Ni^{2+}$ and Co^{2+} [13–15] and in $Me_3Cr_4(PO_4)_6$, $Me = Mg^{2+}$, Zn^{2+} [31]. Compared to Grobunov et al. [7], our data reveal a slightly larger (average *M*(1)–O bond, polyhedral volume) and less distorted *M*(1) site. The most distorted *M*(1) site is found when the Jahn–Teller ions Cu^{2+} and Cr^{2+} are substituted to it. This very well can be seen from the data for the Cr^{3+} containing anhydrous orthophosphates (Table 4). Here the largest OAV (55.3°) is observed for $Cu_3Cr_4(PO_4)_6$, followed by $Cr_3^{2+}Cr_4^{3+}(PO_4)_6$ with OAV = 41.9, whereas the non-Jahn–Teller ions have OAV of $\approx$35°. Generally, the *M*(1) site appears to show a compressed octahedral coordination, which allows the

Table 4
Average bond and edge lengths, polyhedral volumes and distortion parameters for howardevansite-type anhydrous orthophosphate compounds, taken from the literature, in comparison with the data obtained in the present study for the title compound

Compound reference method	Ni_3Fe_4 [13] SX	Co_3Fe_4 [14] RR	Co_3Fe_4 [15] RR	Cu_3Fe_4 [16] RR	Cu_2Fe_5 [16] RR	Fe_3Fe_4 [7] SX	**Fe_3Fe_4 Here SX**	Mn_2Fe_5 [15] RR	Mg_3Cr_4 [31] SX	Zn_3Cr_4 [31] SX	Cu_3Cr_4 [31] SX	Cu_3Cr_4 [32] SX
***M*(1)-site**												
⟨*M*–O⟩ (Å)	2.151	1.169	2.138	2.195	2.136	2.175	2.179	2.194	2.102	2.124	2.199	2.154
⟨O–O⟩ (Å)	3.041	30060	3.022	3.107	3.023	3.075	3.082	3.100	2.970	3.002	3.108	3.050
Volume (Å^3)	13.07	13.32	12.85	13.73	12.71	13.48	13.61	13.77	12.18	12.54	13.79	12.96
BLD (%)	3.90	3.9	3.5	7.1	6.6	4.4	4.2	3.5	3.7	4.5	5.6	7.3
OAV (deg)	30.1	28.9	30.6	35.3	36.9	36.9	27.1	51.3	34.9	36.0	55.3	41.9
OQE	1.0120	1.0121	1.0111	1.0242	1.0201	1.0144	1.0116	1.0164	1.0124	1.0144	1.0223	1.0253
***M*(2)-site**												
⟨*M*–O⟩ (Å)	2.032	2.013	2.002	1.994	2.003	2.001	2.029	2.029	1.987	1.985	1.986	1.985
⟨O–O⟩ (Å)	2.873	2.831	2.814	2.803	2.814	2.828	2.866	2.858	2.803	2.799	2.802	2.801
Volume (Å^3)	10.79	10.45	10.25	10.25	10.26	10.36	10.80	10.79	10.21	10.18	10.20	10.22
BLD (%)	3.9	2.7	2.8	4.0	4.1	4.2	3.5	2.1	1.8	1.9	1.9	2.4
OAV (deg)	83.2	96.1	100.6	92.6	99.9	69.7	68.1	75.4	58.3	56.4	54.0	49.8
OQE	1.0281	1.0288	1.0307	1.0290	1.0320	1.0240	1.0220	1.0220	1.0175	1.0168	1.0161	1.0152
***M*(3)-site**												
⟨*M*–O⟩ (Å)	2.044	2.028	2.066	2.029	2.037	2.044	2.081	2.065	2.033	2.044	2.098	2.098
⟨O–O⟩ (Å)	3.062	3.025	3.066	3.027	3.042	3.047	3.102	3.134	3.042	3.047	3.128	3.031
Volume (Å^3)	6.76	6.52	6.80	6.44	6.55	6.59	6.99	7.18	6.62	6.65	7.03	6.52
BLD (%)	2.3	2.4	3.0	3.1	3.9	2.7	2.1	7.5	1.1	2.1	3.2	3.4
***M*(4)-site**												
⟨*M*–O⟩ (Å)	2.039	1.993	2.029	1.996	1.983	2.018	2.047	2.027	1.982	1.977	1.983	1.972
⟨O–O⟩ (Å)	2.869	2.815	2.869	2.817	2.802	2.839	2.884	2.858	2.803	2.796	2.801	2.787
Volume (Å^3)	10.89	10.14	10.74	10.25	10.06	10.54	11.11	10.43	10.11	10.06	10.22	10.05
BLD (%)	2.9	3.5	4.0	4.0	3.6	2.7	1.8	4.7	2.9	2.8	2.3	2.5
OAV (deg)	84.3	92.7	85.5	75.3	74.6	92.0	70.2	71.9	61.6	55.5	39.1	39.4
OQE	1.0259	1.0292	1.0276	1.0247	1.0249	1.0279	1.0206	1.0247	1.0193	1.0173	1.0121	1.0126
P(1)-site												
⟨P–O⟩ (Å)	1.545	1.532	1.536	1.575	1.581	1.524	1.531	1.521	1.533	1.534	1.526	1.533
⟨O–O⟩ (Å)	2.523	2.499	2.506	2.569	2.580	2.489	2.500	2.482	2.502	2.054	2.491	2.502
Volume (Å^3)	1.89	1.84	1.85	2.00	2.02	1.82	1.84	1.80	1.84	1.85	1.82	1.84
TAV (deg)	7.2	11.7	8.9	12.8	8.2	2.7	2.8	5.7	69	6.9	7.3	8.8
TQE	1.0021	1.0031	1.0026	1.0033	1.0022	1.0007	1.0007	1.0007	1.0019	1.0019	1.0019	1.0024
P(2)-site												
⟨P–O⟩ (Å)	1.549	1.566	1.532	1.552	1.552	1.537	1.538	1.538	1.540	1.540	1.535	1.541
⟨O–O⟩ (Å)	2.528	2.552	2.500	2.533	2.533	2.509	2.511	2.557	2.513	2.512	2.504	2.515
Volume (Å^3)	1.90	1.96	1.84	1.91	1.91	1.86	1.86	1.93	1.87	1.87	1.85	1.87
TAV (deg)	13.4	22.8	14.8	13.8	13.1	5.4	7.2	11.6	13.3	11.5	10.8	10.8
TQE	1.0032	1.0057	1.0037	1.0036	1.0056	1.0015	1.0018	1.0033	1.0032	1.0028	1.0027	1.0026
P(3)-site												
⟨P–O⟩ (Å)	1.550	1.579	1.573	1.544	1.564	1.533	1.535	1.538	1.539	1.539	1.536	1.544
⟨O–O⟩ (Å)	2.531	2.580	2.566	2.522	2.554	2.503	2.507	2.511	2.513	2.512	2.508	2.521
Volume (Å^3)	1.91	2.02	1.99	1.87	1.96	1.85	1.86	1.87	1.87	1.87	1.86	1.88
TAV (deg)	0.7	2.5	6.9	6.3	5.4	2.6	0.6	2.3	2.0	1.2	1.5	1.5
TQE	1.0004	1.0020	1.0017	1.0019	1.0019	1.0008	1.0003	1.0008	1.0009	1.0006	1.0007	1.0008

RR = Rietveld method. SX = single-crystal X-ray diffraction;

BLD (bond lengths distortion) $= \frac{100}{n}\sum_{i=1}^{n}\frac{|(X-O)_i - (\langle X-O\rangle)|}{(\langle X-O\rangle)}$ %, where n is the number of bonds and (X–O) is the central cation–oxygen length;

ELD (edge lengths distortion) $= \frac{100}{n}\sum_{i=1}^{n}\frac{|(O-O)_i - (\langle O-O\rangle)|}{(\langle O-O\rangle)}$ %, where n is the number of bonds and (O–O) is the polyhedron edge length;

OAV (octahadral angle variance) $= \sum_{i=1}^{12}(\Theta_i - 90)^2/11$; TAV (tetrahedral angle variance) $= \sum_{i=1}^{n}(\Theta_i - 109.47)^2/5$.

stabilization of Jahn–Teller ions such as Cu^{2+} and Cr^{2+} [31]. The average $M(1)$–O bond lengths roughly correlate with the increasing size of the cations on $M(1)$. This is more evident for Cr^{3+} containing samples [31,32] than for the Fe^{3+} bearing ones [7,13–15].

The $M(3)$ site, also hosting divalent cations and having the trigonal bi-pyramidal oxygen coordination, shows less bond length distortion. The average M(3)–O bond length (2.081 Å) found for the title compound is distinctly larger than the one given by Grobunov et al. [7]. Also, the average of the O–O distances forming the edges of the coordination polyhedron, as well as the coordination polyhedral volume is distinctly smaller in Ref. [7]. These observations might be due to some ferric iron on the $M(3)$ site in the compound of Ref. [7].

The $M(2)$ and the $M(4)$ sites host the trivalent cations in the howardevansite-type anhydrous orthophosphates. Comparing our data to the ones of Grobunov et al. [7], we find similar octahedral distortion but somewhat larger average bond and edge lengths and octahedral site volumes for the $M(2)$ site. For the $M(4)$ we observe distinctly larger average bond and edge lengths, the octahedral volume is larger by nearly 0.6 $Å^3$, whereas the octahedral angle variance is smaller by $\approx 25\%$. It is evident from Table 4, that the title compound exhibits the most regular $M(2)$ and $M(4)$ sites among the known iron containing howardevansite-type orthophosphates. The average $M(2)$–O and $M(4)$–O bond lengths in the Cr^{3+} containing compounds are slightly shorter than the Fe^{3+} bearing compounds, and remain remarkably constant with changing chemical composition of the neighboring $M(1)$ and $M(3)$ sites. This especially is evident for the $M(2)$ site. Here all structural parameters remain quite constant (Table 4). Generally, the $M(2)$ and the $M(4)$ sites are closer to the geometry of an ideal octahedron in the $Me_3^{2+}Cr_4^{3+}(PO_4)_6$ compounds than in the $Me_3^{2+}Fe_4^{3+}(PO_4)_6$ ones (smaller OAV, similar BLD).

The structural parameters for the PO_4 tetrahedra in the title compound are similar to the ones reported previously by Grobunov et al. [7]. For all compounds listed in Table 4, the average bond lengths range between 1.53 and 1.58 Å, the tetrahedral volume is between 1.80 and 2.00 $Å^3$. The data are remarkably similar for the Cr^{3+} containing samples (cf. Table 4), but are somewhat diverse for the Fe^{3+}-containing compounds. However, this spread is most probably due to the lower precision of the Rietveld-method derived data than it is a real intrinsic structural effect. This is concluded from the remarkable constancy of the data for the Cr^{3+}-containing samples, having similar ($M1$) and $M(3)$ cationic compositions. A feature observed for the P-sites in title compound is of a more general nature. It concerns the distortion of the tetrahedral sites, which is smallest for the P(3) site, and largest for the P(2) site. As observed for the M-sites, also the P-sites show small tetrahedral distortion when compared to the other compounds (Table 4).

3.5. ^{57}Fe Mössbauer spectroscopy

At room temperature, the ^{57}Fe Mössbauer spectrum exhibits three broad resonance absorption lines, which result from a superposition of four different subspectra (Fig. 4a). The line at a Doppler velocity of ≈ 2.4 mm/s is due to Fe^{2+} and shows an distinct shoulder, which can be regarded as a clear evidence for two different Fe^{2+} doublets. Furthermore, the resonance absorption line at ≈ 0.8 mm/s, which is due to Fe^{3+}, is too wide to be due to a single doublet, thus two different ferric subspectra have to be assumed. The broad line at ≈ 0.0 mm/s, which additionally shows some structure at the bottom end, is a superposition of four different subspectra. After full thickness correction [25] of the raw-data, a full static hyperfine interaction Hamiltonian site analysis was performed using 4 Lorentzian shaped doublets. The

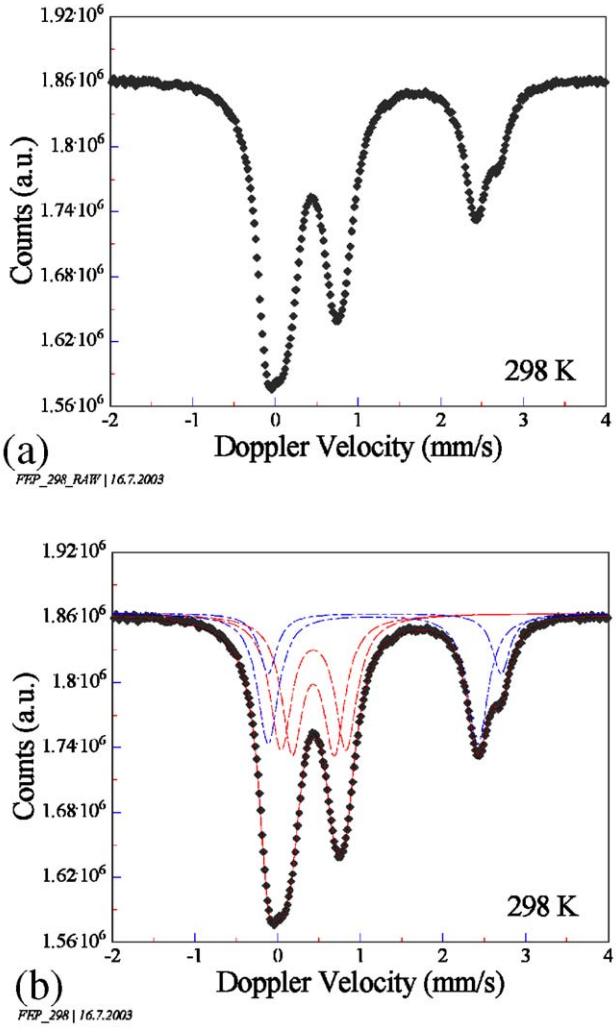

Fig. 4. ^{57}Fe Mössbauer spectra of the title compound (a) raw spectrum at 298 K, (b) thickness corrected and refined spectrum at 298 K.

refinement yields a perfect mathematical description of the experimental data (Fig. 4b) and leads to ^{57}Fe hyperfine parameters, which can be found in Table 5.

The four different doublets (two for Fe^{2+} and two for Fe^{3+}) can be related to the four different crystallographic sites of the title compound. The assignment of the two Fe^{2+} doublets is trivial as the relative area ratio shows a 2:1 stoichiometry in the Mössbauer spectrum in accordance with the crystal structure. Thus, the doublet with the large isomer shift (δ) of 1.29(1) mm/s and a quadrupole splitting (Δ) of 2.82(2) mm/s (values at 298 K) is assigned to the Fe(1) site, the doublet with $\delta = 1.154(5)$ mm/s and $\Delta = 2.54(1)$ mm/s (298 K data) to the 5-fold coordinated Fe(3) site. The assignment is not only reasonable because of the relative site areas, but also because of the general observation, that the isomer shift decreases with decreasing coordination number [33]. Indeed the 5-fold coordinated Fe(3) site shows the smaller isomer shift ($\delta = 1.15(1)$ mm/s) as compared to the Fe(1) site ($\delta = 1.29(1)$ mm/s). The ^{57}Fe hyperfine parameters for Fe^{2+} found in this study are in good agreement with the ones found previously on the title compound [34,35], that is $\delta = 1.34(1)$ mm/s and $\Delta = 2.85(2)$ mm/s for the 6-fold coordinated Fe(1) site and $\delta = 1.15(1)$ mm/s and $\Delta = 2.60(2)$ mm/s for the 5-fold coordinated Fe(3) site [35]. Polyhedral distortion can be related to the magnitude of the quadrupole splitting [36]. For octahedral Fe^{2+}, the QS generally decreases with increasing deviation of the electronic/geometric environment around the Fe nucleus from cubic point symmetry [31,34]. Thus the electronic/geometric environment around the 5-fold coordinated Fe(3) site ($\Delta = 2.54$ mm/s at 298 K) can be regarded as being more distorted than the one around the Fe(1) site ($\Delta = 2.82$ mm/s at 298 K). Furthermore, the rather large quadrupole splitting of Fe(1) at 298 K indicates that the Fe(1) site possess a rather regular electronic/geometric local environment around the Fe-nucleus.

Table 5
^{57}Fe Mössbauer parameters of $Na_{0.10}Fe^{2+}_{3.11}Fe^{3+}_{3.88}(PO_4)_6$ at different temperatures, derived from thickness corrected spectra.

	295 K	240 K	180 K	120 K	80 K
δ	1.293(5)	1.351(3)	1.386(4)	1.434(4)	1.443(4)
Δ	2.820(7)	2.821(8)	2.863(7)	2.882()	2.861(5)
Γ	0.256(9)	0.231(8)	0.252(8)	0.230(7)	0.236(8)
A	14.5(5)	13.4(5)	14.2(5)	14.2(6)	13.9(6)
Site	Fe^{2+} [Fe(1)]				
δ	1.153(5)	1.190(6)	1.215(6)	1.257(6)	1.273(6)
Δ	2.538(6)	2.616(6)	2.658(7)	2.687(6)	2.682(6)
Γ	0.302(6)	0.234(7)	0.242(7)	0.242(8)	0.238(7)
A	28.6(5)	28.5(6)	28.5(6)	29.1(5)	28.9(6)
Site	Fe^{2+} [Fe(3)]				
δ	0.434(6)	0.477(5)	0.515(5)	0.546(6)	0.540(5)
Δ	0.521(6)	0.520(6)	0.521(6)	0.516(7)	0.515(6)
Γ	0.308(6)	0.262(8)	0.268(8)	0.260(8)	0.256(7)
A	28.4(6)	28.9(6)	28.8(5)	28.3(5)	28.6(5)
Site	Fe^{3+} [Fe(4)]				
δ	0.435(9)	0.480(5)	0.510(6)	0.545(5)	0.541(7)
Δ	0.792(5)	0.804(6)	0.812(5)	0.819(4)	0.822(5)
Γ	0.316(7)	0.257(6)	0.260(6)	0.258(6)	0.256(6)
A	28.5(6)	29.3(5)	28.3(7)	28.4(5)	28.7(6)
Site	Fe^{3+} [Fe(2)]				
χ^2	1.498	1.439	1.913	1.412	1.792

δ = isomer shift (mm/s), Δ = quadrupole splitting (mm/s), Γ = full-width at half-maximum (mm/s), A = relative area ratio.

The assignment of the two ferric iron doublets is not as straightforward as the one of the ferrous doublets. In contrast to Fe^{2+} ($3d^6$ configuration), Fe^{3+} possesses a spherical electronic charge distribution around the nucleus ($3d^5$ configuration). Thus for Fe^{3+} the dominating contribution to the electric field gradient (and consequently to the quadrupole splitting) is the lattice term, the valence term is generally very small. Thus, polyhedral distortion can be directly related to geometric distortion of the corresponding Fe^{3+} site. Structure analysis has shown that the two Fe^{3+} octahedral sites are rather similar. The Fe(4) site appears to have a slightly smaller bond length distortion (BLD) as compared to the Fe(2) site. The OAV and the OQE parameters are quite similar. For a tentative assignment, the doublet with the isomer shift of $\delta = 0.434(6)$ mm/s and with the smaller quadrupole splitting of $\Delta = 0.522(6)$ mm/s is related to Fe(4) site, the one with $\delta = 0.435(9)$ mm/s and $\Delta = 0.792(2)$ mm/s to the Fe(2) site.

Additional information is needed, which can be gained from the temperature dependence of the quadrupole splitting Δ. In contrast to Fe^{2+}, the temperature-dependent variation of Δ Fe^{3+} is small, and arises from changes in the lattice contribution to the electric field gradient. Thus, changes are directly related to changes in the geometry of the oxygen polyhedron around the Fe^{3+} cation. The changes of Δ Fe^{3+} for the title compound indeed are small, however, some systematic variation can be found (Fig. 5, Table 5).

Although the overall changes are very small, the quadrupole splitting of Fe^{3+} on the Fe(4) site slightly decreases with decreasing temperature, thus the Fe(4) site should be slightly more regular in terms of polyhedral distortion parameters at low temperatures. This is actually the case, as e.g., the BLD decreases by $\approx 0.1\%$ and the OAV decreases by $\approx 1^\circ$ (Table 3). For Fe^{3+} on the Fe(2) site, the increase of quadrupole splitting with decreasing temperature suggests an increase of polyhedral distortion. This is actually the case (Table 3). Thus, the assignment of Fe^{3+} doublets is assumed to be correct.

The ^{57}Fe hyperfine parameters for Fe^{3+} found in this study are quite similar to the data given in literature [34,35]. Belik et al. [35] gave values of $\Delta = 0.57(2)$ and 0.82(2) mm/s, Gleitzer [34] found $\Delta = 0.53$ and 0.83 mm/s

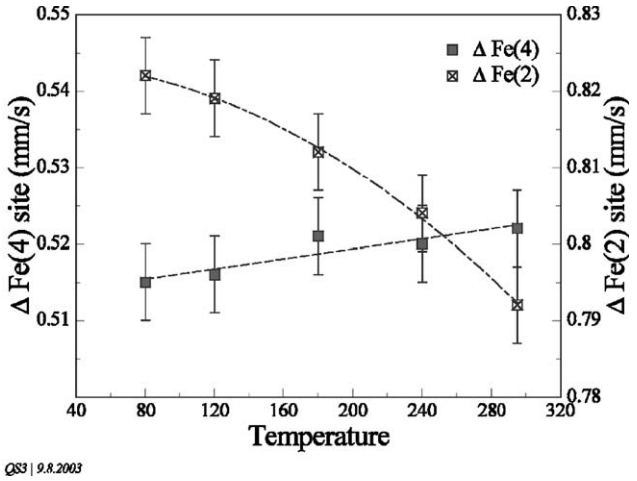

Fig. 5. Variation of the quadrupole splitting of Fe^{3+} in $Na_{0.10}Fe^{2+}_{3.11}Fe^{3+}_{3.88}(PO_4)_6$.

(no errors given) for the two Fe^{3+} subspectra. However, no site assignment was given in the two references. Based on the combination of precise structural parameters and temperature-dependent variation of ^{57}Fe hyperfine parameters it was possible to give a doublet assignment also for ferric iron in the present study. ^{57}Fe Mössbauer spectroscopy has also been used to characterize $Ni_3Fe_4(PO_4)_6$ [13] and $Cu_{3-x}Fe_{4+x}(PO_4)_6$ [16], but again, no doublet assignment has been made for Fe^{3+}. Based on the above suggestion, to dedicate the doublet with the smaller quadrupole splitting to the $M(4)$ site, the one with the larger quadrupole splitting to the $M(2)$ site, and using the distortion parameters OAV and BLD, one finds that in all cases, the larger quadrupole splitting value is associated with the larger OAV and the larger BLD value (Table 4). In $Fe_3Fe_4(PO_4)_6$, we find small quadrupole splittings of 0.51 and 0.79 mm/s for $M(4)$ and $M(2)$, respectively, whereas for $Ni_3Fe_4(PO_4)_6$ values of 0.61 and 1.00 mm/s are reported [13]. The larger quadrupole splittings correlate very well with the larger polyhedral distortion in $Ni_3Fe_4(PO_4)_6$ (Table 4) and further support our doublet assignment. The data on $Cu_{3-x}Fe_{4+x}(PO_4)_6$ [16] plot very well into the described trend.

4. Summary

(i) Between 673 and 773 K, the hydrothermal treatment of synthetic barbosalite resulted in the anhydrous mixed valence compound $Na_{0.10}Fe^{2+}_{3.11}Fe^{3+}_{3.88}(PO_4)_6$. At high temperatures, the ferrous iron compound $Fe^{2+}_2P_2O_7$ is stabilized.

(ii) $Na_{0.10}Fe^{2+}_{3.11}Fe^{3+}_{3.88}(PO_4)_6$ is triclinic, P-1. The main structural building unit is a buckled crankshaft-like chain, passing through the unit cell in [101] direction. The chain is built up by the oxygen coordination polyhedra around the Fe(2), Fe(3) and the Fe(4) cation via shared edges. Within such a chain, pairs of Fe^{3+} are interrupted by one Fe^{2+} cation. Ferric iron occupies two octahedral sites, which are rather similar in terms of polyhedral distortion. Ferrous iron is found at the center of inversion at $(\frac{1}{2}, \frac{1}{2}, \frac{1}{2})$, where it is 6-fold coordinated and one 5-fold coordinated site. To the authors' best knowledge, Fe^{2+} in 5-fold coordination is rather rare. The buckled chains are related to each other via the center of inversion at $(\frac{1}{2}, \frac{1}{2}, \frac{1}{2})$. On basis of the long interatomic Fe–Fe distances and the ordered arrangement of Fe^{2+} and Fe^{3+} it is assumed that no thermally induced electron charge transfer at elevated temperatures will take place.

(iii) In terms of polyhedral distortion parameters the title compound represents the most regular howardevansite-type Fe-containing orthophosphate. More generally spoken, it is among the most regular anhydrous orthophosphate compounds reported so far to show the howardevansite-structure type. Thus the structure of $Fe_7(PO_4)_6$ may be described as the low distorted aristo-type of this structural orthophosphate family.

(iv) ^{57}Fe Mössbauer spectra show four components, two for Fe^{2+} and two for Fe^{3+}. On basis of polyhedral distortion and the temperature evolution of quadrupole splitting it is possible to relate to the four different Fe sites of the structure.

Acknowledgments

GJR wishes to thank the Austria Academy of Science for financial support via an APART (Austrian Program for Advanced research and technology) scholarship in 2000–2003.

References

[1] G. Amthauer, G.R. Rossmann, Phys. Chem. Minerals 11 (1984) 37.
[2] R. Bauminger, S.G. Cohen, A. Marinov, S. Ofer, E. Segal, Phys. Rev. 122 (1961) 1447.
[3] F.J. Litterst, G. Amthauer, Phys. Chem. Minerals 10 (1984) 250.
[4] B.J. Evans, G. Amthauer, Phys. Chem. Solids 41 (1980) 985.
[5] J.M.M. Millet, D. Rouzies, J.C. Vedrine, Appl. Catal. A 124 (1995) 205.
[6] E. Kral, Doctoral Thesis, University Salzburg, 1992.
[7] Yu.A. Grobunov, B.A. Maksimov, Yu.K. Kabalov, A.N. Ivashenko, O.K. Mel'nikov, N.V. Belov, Dokl. Akad. Nauk. SSSR 254 (1980) 873.
[8] J.M. Hughes, J.W. Drexler, C.F. Campana, M.L. Malinconico, Am. Mineral. 73 (1988) 181.
[9] A.A. Belik, Mater. Res. Bull. 34 (1999) 1973–1980.

[10] M.A. Lafontaine, J.M. Greneche, Y. Laligant, G.J. Ferey, Solid State Chem. 108 (1994) 1.
[11] C. Gicquel-Mayer, M. Mayer, G. Perez, Acta Crystallogr. B 37 (1981) 1035.
[12] R.F. Klevtsova, V.G. Khim, P.V. Klevtsov, Kristallografiya 25 (1980) 1148.
[13] A. El Kira, R. Gerardin, B. Malaman, C. Gleitzer, Eur. J. Solid State Inorg. Chem. 29 (1992) 1119.
[14] M.R. De Guire, T.R.S. Prasanna, G. Kalonji, R.C. O'Handley, J. Am. Ceram. Soc. 70 (1987) 831.
[15] P. Lightfood, A.K. Cheetham, J. Chem. Soc. Dalton Trans. 1989 (1989) 1765.
[16] A.A. Belik, A.P. Malakho, K.V. Pokholok, B.I. Lazoryak, S.S. Khasanov, J. Solid State Chem. 150 (2000) 159.
[17] R. Vochten, E. DeGrave, Phys. Chem. Minerals 7 (1981) 197.
[18] H. Eugster, D.R.J. Wones, J. Petrol. 3 (1962) 82.
[19] Stoe & Cie X-SHAPE and X-RED: Programs for optimisation of the crystal shape (w.r.t the merging *R*-value) and numerical absorption correction, Stoe & Cie, Darmstadt, Germany, 1996.
[20] G.M. Sheldrick, SHELXS-97, Program for crystal structure solution, University of Göttingen, Germany, 1997.
[21] G.M. Sheldrick, SHELXL-97, Program for crystal structure refinement, University of Göttingen, Germany, 1997.
[22] L.J.J. Farrugia, J. Appl. Crystallogr. 32 (1999) 837.
[23] A.J.C. Wilson (Ed.), International Tables for Crystallography, Vol. C, Kluwer Academic Publishers, Dordrecht, The Netherlands, 1992.
[24] K. Brandenburg, M.J. Berndt, J. Appl. Crystallogr. 32 (1999) 1028.
[25] D.G. Rancourt, A.M. McDonald, A.E. Lalonde, J.A. Ping, Am. Mineral. 78 (1993) 1.
[26] D.G. Rancourt, J.Y. Ping, R.G. Berman, Phys. Chem. Minerals 21 (1996) 258.
[27] D.G. Rancourt, J.Y. Ping, Nucl. Instrum. Methods: Phys. Res. B 58 (1992) 85.
[28] K. Robinson, G.V. Gibbs, P.H. Ribbe, Science 172 (1971) 567.
[29] N.E. Brese, M. O'Keeffe, Acta Crystallogr. B 47 (1991) 192.
[30] R.E. Shannon, C.T. Prewitt, Acta Crystallogr. B 25 (1968) 925.
[31] M. Gruss, R. Glaum, Z. Kristallogr. 212 (1997) 510.
[32] R. Glaum, Z. Kristallogr. 205 (1993) 69.
[33] D. Barb, Grundlagen and Anwendung der Mössbauer Spektroskopie, Akademie Verlag, Berlin, 1980, 467pp.
[34] C. Gleitzer, Eur. J. Solid State Inorg. Chem. 28 (1991) 77.
[35] A.A. Belik, A.P. Malakho, K.V. Pokholok, B.I. Lazoryak, Russ. J. Inorg. Chem. 44 (9) (1999) 1535.
[36] R. Ingalls, Phys. Rev. A 133 (1964) 787.